PNAS
www.pnas.org

Supplementary Information for

Abrogation of pre-nucleation, transient oligomerization of the Huntingtin exon-1 protein by human profilin-I

Alberto Ceccon[a], Vitali Tugarinov[a], Rodolfo Ghirlando[b] and G. Marius Clore[a]

[a]Laboratory of Chemical Physics, National Institute of Diabetes and Digestive and Kidney Diseases, National Institutes of Health, Bethesda, Maryland 20892-0520

[b]Laboratory of Molecular Biology, National Institute of Diabetes and Digestive and Kidney Diseases, National Institutes of Health, Bethesda, Maryland 20892-0540

www.pnas.org/cgi/doi/10.1073/pnas.1922264117

SI Materials and Methods

Expression and purification of htt^{ex1} and htt$^{NT}Q_7P_{11}K_2$ peptides. Both htt^{ex1} and htt$^{NT}Q_7P_{11}K_2$ peptides were expressed as fusion proteins, with the immunoglobulin-binding domain of streptococcal protein G (GB1) attached to the peptide N-termini, following a protocol described previously (1, 2). Codon optimized htt^{ex1} and htt$^{NT}Q_7P_{11}K_2$ gene constructs cloned in pET-21d(+) plasmids with NcoI and BamHI cloning sites, were purchased from Genscript Inc. (Piscataway, NJ). Both plasmids contained a 6 Histidine (His_6) tag following the sequence of GB1 and prior to the Factor Xa cleavage site (GB1 – His_6 – FXa cleavage site - peptide). The GB1-htt^{ex1} and GB1-htt$^{NT}Q_7P_{11}K_2$ fusion constructs were expressed in *E. Coli* BL21 (DE3) cells grown in M9 minimal medium supplemented with appropriate ^{15}N and/or ^{13}C isotope sources. Uniform ^{15}N and ^{13}C labeling was achieved by using $^{15}NH_4Cl$ and $^{13}C_6$-D-glucose as the sole nitrogen and carbon sources, respectively. Fractional $^{13}C\alpha$ labeling (with all other carbons at natural isotopic abundance) was achieved using [2-^{13}C]-D-glucose as the sole carbon source (3). This labeling strategy produces proteins selectively fractionally $^{13}C\alpha$-labeled in all residues except leucine (where the Cα position is labeled at less than 10%), and isoleucines and valines (where $^{13}C\alpha$-$^{12}C\beta$ and $^{13}C\alpha$-$^{13}C\beta$ pairs are in a ration of 1.2:1) (3). Following protein over-expression (at 20 °C for 18 h), the cells were harvested by centrifugation (4,500 × g for 25 min), and the resulting cell pellet resuspended in buffer comprising 50 mM Tris-HCl, pH 8, 100 mM NaCl and 20 mM imidazole. EDTA-free protease inhibitors (Roche Life Science) were added to the suspension, and the cells were lysed by heating to 80°C for 10 min. The cell lysate was clarified by centrifugation (40,000 × g for 25 min). The His-tagged fusion proteins were subsequently isolated by affinity chromatography using a HisTrap HP 5 ml column (GE Healthcare, USA) on an AKTA explorer FPLC system. The GB1 fusion domain and the associated His_6 tag were cleaved by addition of Factor Xa (0.0065 mg/mL) directly to the fractions containing the eluted proteins, and the excess imidazole eliminated by extensive dialysis against buffer containing 50 mM Tris-HCl, pH 8, 100 mM NaCl, 20 mM imidazole for 18 h (4 °C). The GB1-His_6 tag was subsequently removed from the solution by affinity chromatography. The htt^{ex1} and htt$^{NT}Q_7P_{11}K_2$ polypeptides were purified by reverse phase high performance liquid chromatography (HPLC) using a preparative scale C4 column (Vydac) as described previously (2). Both peptides were eluted with a gradient (from 20 to 45 %) of solvent B (95% v/v acetonitrile, 4.9% v/v H_2O, 0.1% v/v trifluoroacetic acid (TFA)) in solvent A (5% v/v acetonitrile, 94.9% v/v H_20 and 0.1% v/v TFA). Following purification, a disaggregation procedure involving the dissolution of the peptides in a 1:1 (v/v) mixture of TFA and hexafluoroisopropanol (HFIP) (4), was used to ensure complete removal of any pre-existing aggregates that can potentially accelerate aggregation of monomeric peptides. The TFA:HFIP solvent mixture was removed under a stream of N_2 gas directed into the flask through a glass pipette for 4 h. The peptide film was then dissolved in 0.1 mM TFA prior to lyophilization. Completion of the cleavage reaction and the peptide identity were confirmed by liquid phase chromatography coupled with electrospray mass spectrometry (LC-MS).

Expression and purification of human profilin-I. Recombinant human profilin-I (referred to hereafter as profilin) was expressed and purified as described in (5). *E.coli* cells were transformed with the pET-15b plasmid containing the PFN1 gene bearing an N-terminal His-tag, and grown at 37 °C either in M9 minimal medium, containing $^{15}NH_4Cl$ and $^{12}C_6$-D-glucose as the sole nitrogen and carbon sources, respectively, or in Luria-Bertani (LB) rich medium. Following protein over-expression for 4 h at 37 °C, the cells were harvested, resuspended in buffer (20 mM sodium phosphate, pH 6.5, 150 mM NaCl, 20 mM imidazole and 2 mM dithiothreitol (DTT)), and sonicated. The cell debris was removed by centrifugation (40,000 × g for 25 min), the supernatant injected onto a HisTrap HP 5 ml column (GE Healthcare, USA), and the protein

eluted using a step gradient of imidazole (20 to 500 mM). The His-tag was subsequently removed by overnight proteolysis with tobacco etch virus (TEV) protease in 20 mM phosphate buffer, pH 6.5, 150 mM NaCl and 2 mM DTT. The last step of purification consisted of gel filtration on a Superdex 75 column, followed by dialysis against a buffer comprising 20 mM phosphate, pH 6.5, 50 mM NaCl, 2 mM DTT and 1 mM EDTA.

Preparation of NMR samples. NMR samples of huntingtin peptides were prepared by dissolving an aliquot of the htt^{ex1} or $htt^{NT}Q_7P_{11}K_2$ polypeptides in a 13.8 mM monobasic sodium phosphate buffer, pH 4.6, containing 50 mM NaCl in 10% D_2O/90% H_2O (v/v). As described previously, lower pH improves peptide solubility (4). The pH of the buffer was subsequently adjusted to 6.5 by adding dibasic sodium phosphate for a final sodium phosphate concentration of 20 mM. The concentration of the htt^{ex1} and $htt^{NT}Q_7P_{11}K_2$ polypeptide stock solutions was 1.5 mM, and the stocks were diluted to the appropriate final concentrations prior to NMR measurements. NMR samples containing profilin were dissolved in a 20 mM monobasic sodium phosphate buffer, pH 6.5, containing 50 mM NaCl, 2 mM DTT and 1 mM EDTA in 10 % D_2O/90 % H_2O (v/v).

Sedimentation velocity analytical ultracentrifugation. Sedimentation velocity experiments were carried out on a Beckman Optima XL-A or Beckman Coulter ProteomeLab XI-I analytical ultracentrifuge at 50,000 or 60,000 rpm (10 °C) following standard protocols (6). Samples of htt^{ex1}, prepared in 20 mM sodium phosphate buffer, pH 6.5, 50 mM NaCl and 10% D_2O /90 % H_2O (v/v), were analyzed at a series of protein concentrations ranging from 0.2 to 1.2 mM. The samples were loaded into 3 mm path-length, 2-channel centerpiece cells, and sedimentation data were collected using the absorbance and interference optical detection systems. Time-corrected data (7, 8) were analyzed in SEDFIT 16.1c (9) in terms of a continuous c(*s*) distribution of sedimenting species (Fig. S1). The solution density and viscosity were measured on an Anton Paar DMA 5000 density meter and Anton Paar AMVn automated rolling ball viscometer, respectively, at 20 °C and corrected to 10 °C. The protein partial specific volume was determined based on the composition in SEDNTERP (10). Sedimentation coefficients were corrected to $s_{20,w}$ values at standard conditions.

NMR spectroscopy. All NMR experiments were recorded at 5 °C (with the exception of 3D triple resonance experiments for backbone resonance assignments that were performed at 10 °C) using Bruker Avance-III spectrometers, equipped with TCI triple resonance *z*-axis gradient cryogenic probes operating at ^{1}H Larmor frequencies of 900.16, 800.13 and 600.82 MHz. Backbone ^{1}H, ^{13}C and ^{15}N resonance assignments of htt^{ex1} were carried out using standard 3D triple resonance HNCACB AND CBCA(CO)NH experiments on a 0.5 mM ^{15}N/^{13}C-labeled sample of htt^{ex1}. The NMR data were processed using NMRPipe (11), and in the case of exchange induced shift measurements, the time domain in the indirect dimension (^{15}N or ^{13}C) was extended two-fold through the application of sparse multidimensional iterative lineshape-enhanced (SMILE) reconstruction (12). The backbone assignments for htt^{ex1} have been deposited in the Biological Magnetic Resonance Bank (www.bmrb.wisc.edu; BMRB accession codes 50122).

^{15}N/^{13}Cα-CPMG relaxation dispersion experiments. All ^{15}N-CPMG relaxation dispersion experiments were recorded using a pulse scheme that provides the effective relaxation rates of in-phase ^{15}N coherences (13), with amide proton decoupling during the relaxation period achieved by continuous wave (CW) irradiation using a radio frequency (RF) field strength of 11 kHz. Reference experiments for all ^{15}N-CPMG

measurements were obtained by omitting the relaxation period. ^{15}N-CPMG relaxation dispersion experiments on 0.8, 0.6 and 0.3 mM ^{15}N/^{13}Cα-labeled htt^{ex1} were recorded at 600 and 900 MHz with the relaxation period set to 100 ms, and the following CPMG fields (ν_{CPMG}): 0, 10, 20, 40, 70, 90, 110, 130, 150, 180, 210, 240, 280, 320, 420, 500, 580, 660, 740, 820, 900 and 1000 Hz. ^{15}N-CPMG relaxation dispersion experiments on 0.75 and 0.4 mM ^{15}N/^{13}C-labeled htt^{ex1} in the presence of 4.8 mM unlabeled profilin were recorded at 600 and 800 MHz with the relaxation period set to 80 ms and the following set of CPMG fields: 0, 12.5, 25, 50, 75, 100, 125, 150, 200, 225, 275, 325, 375, 437.5, 500, 562.5, 625, 750, 875 and 1000 Hz. ^{15}N-CPMG relaxation dispersion measurements on 0.4 mM ^{15}N/^{13}C-labeled profilin in the presence of 15 μM unlabeled htt^{NT}Q$_7$P$_{11}$K$_2$ were recorded at 600 and 800 MHz, with the relaxation period set to 30 ms and the following CPMG fields: 0, 33.3, 66.7, 100.0, 133.3, 166.7, 233.3, 300, 366.7, 433.3, 500, 600, 666.7, 800, 933.3 and 1000.0 Hz.

^{13}Cα-CPMG relaxation dispersion experiments were recorded using the pulse scheme described in (14) with ^{1}Hα CW decoupling during the relaxation period applied with a RF field strength of 12 kHz. The reference experiments were obtained by omitting the relaxation period. ^{13}Cα-CPMG relaxation dispersion experiments on 0.8, 0.6 and 0.3 mM ^{15}N/^{13}Cα-labeled htt^{ex1} were recorded at 600 and 900 MHz with the ^{13}Cα relaxation period set to 40 ms and the following set of CPMG fields: 0, 25, 50, 75, 100 ,125, 150, 200, 250, 300, 400, 500, 600, 750, 925, 1125, 1375, 1675 and 2000 Hz. ^{13}Cα-CPMG relaxation dispersion experiments on 1.0 mM ^{15}N/^{13}Cα-labeled htt^{NT}Q$_7$P$_{11}$K$_2$ in the presence of 0.1 mM unlabeled profilin were recorded at 600 and 800 MHz with the relaxation period set to 30 ms and the following CPMG fields: 0, 33.3, 66.7, 100.0, 133.3, 166.7, 200.0, 266.7, 333.3, 400.0, 533.3, 666.7, 866.7, 1000.0, 1166.7, 1333.3, 1500.0, 1666.7, 1833.3 and 2000 Hz.

^{15}N transverse spin relaxation rate (R_2) and lifetime line-broadening (ΔR_2) measurements. The values of ^{15}N-R_2 for 0.1 mM ^{15}N-labeled htt^{ex1} in the absence and presence of profilin were obtained from the measured ^{15}N-$R_{1\rho}$ (1.5 kHz spin-lock field) and ^{15}N-R_1 rates at 600 MHz and 5 °C using the pulse schemes and procedures described previously (2, 15). Lifetime line-broadening (^{15}N-ΔR_2) values (Fig. 4B, main text) were calculated as the difference between ^{15}N-R_2 values of htt^{ex1} obtained in the presence and absence of profilin.

^{13}Cα and ^{15}N exchange-induced chemical shifts (δ_{ex}). The concentration-dependent changes in ^{13}Cα and ^{15}N chemical shifts of ^{15}N/^{13}C-labeled htt^{ex1} were obtained from 2D ^{1}H-^{13}C constant-time (CT)-HSQC (900 MHz) and 2D ^{1}H-^{15}N HSQC (800 MHz) spectra, respectively, recorded in the absence and presence of profilin. A constant-time period of 56 ms (~ $2/J_{CC}$) was used in the 2D ^{1}H-^{13}C CT-HSQC experiments. Successive dilutions of ^{15}N/^{13}C-labeled htt^{ex1} from the 1.2 mM to 50 μM concentration were performed by addition of NMR buffer (20 mM phosphate buffer, pH 6.5, 50 mM NaCl and 90% H_2O/10 % D_2O v/v), with the protein concentration and pH verified at each dilution step. ^{13}Cα and ^{15}N exchange-induced chemical shifts (δ_{ex}) were calculated as, $\delta_{ex}(i) = \delta_{obs}(i) - \delta_{ref}$, where δ_{obs} is the observed chemical shift at the peptide concentration i, and δ_{ref} is the chemical shift at a concentration of 50 μM htt^{ex1}. The errors in peak positions were determined as described earlier (2). The absence of any observable changes in ^{13}Cα chemical shifts of Thr2, Gln22 and Gln23 and the ^{15}N shift of His71 are indicative of the pH stability and continuity of conditions of the NMR samples over the entire concentration range. For the measurements of δ_{ex} in the presence of unlabeled profilin, the concentration of profilin was kept constant throughout at 4.8 mM by including profilin in the NMR buffer. The changes in ^{15}N chemical shifts of the 0.4 mM ^{15}N/^{13}C-labeled profilin in the presence of 15 μM htt^{NT}Q$_7$P$_{11}$K$_2$ were obtained from 2D ^{1}H-^{15}N HSQC spectra recorded at

600 and 800 MHz. ^{15}N-δ_{ex} values were obtained in the same manner as for htt^{ex1} but using the chemical shifts of free profilin as the reference, $\delta_{ref.}$

Quantitative analysis of pre-nucleation transient oligomerization of free htt^{ex1}. The characterization of the inter-conversion between free monomeric htt^{ex1} and several oligomeric htt^{ex1} species followed closely that of our previous study of transient oligomerization of the shorter huntingtin variant, htt^{NT}Q$_7$ (2) from both experimental and analytical perspectives. The reader is referred to the *SI Appendix* of (2), where the details of data analysis, the assumptions used in the modeling of the oligomerization kinetics, as well as the procedures of model selection, are discussed at length. Similar sets of concentration-dependent ^{15}N/^{13}Cα CPMG relaxation dispersion and ^{15}N/^{13}Cα exchange-induced shift data were collected for htt^{ex1} as were obtained and analyzed previously for the shorter htt^{NT}Q$_7$ variant (see 'Materials and Methods' above). All the experimental data used for analysis is shown in Fig. S2. The data were included into the minimized target function consisting of the differences squared between experimental and calculated values of each observable (2). The minimal oligomerization model that accounts for all the data, comprising an on-pathway dimer (**E$_2$**) and tetramer (**E$_4$**), and an off-pathway dimer (**E$_2^*$**) which does not undergo further oligomerization, is summarized in Fig. 2D of the main text. The Δω values are listed in Table S1.

To test the robustness of the global fit to all the CPMG relaxation dispersion and δ_{ex} data, we also carried out the following set of calculations: since chemical exchange for the on-pathway process is fast on the chemical shift time scale, the δ_{ex} data were fit independently based simply on optimizing the Δω values and equilibrium dissociation constants for the on-pathway process only. These optimized parameters were then held fixed, and the CPMG relaxation dispersion data were best-fit including the off-pathway dimer. This procedure, which is significantly faster computationally than the full global minimization, yielded essentially the same results as the full global minimization against the CPMG relaxation dispersion and δ_{ex} data simultaneously.

Quantitative analysis of profilin-htt^{ex1} binding. The set of coupled equilibria describing the binding of profilin to the two distinct polyproline binding sites of htt^{ex1}, P$_{11}$ and P$_{10}$, is shown in Fig. 4D and described in the main text. Here, we reproduce for convenience the binding scheme used for analysis of δ_{ex} and R_2 titration data obtained for each binding partner (Scheme S1), and describe how fractional populations p_i of each complex i ($i \in$ {**PE**, **PE′**, **P$_2$EE′**}) in Fig. 4D and Scheme S1 can be obtained from material balance.

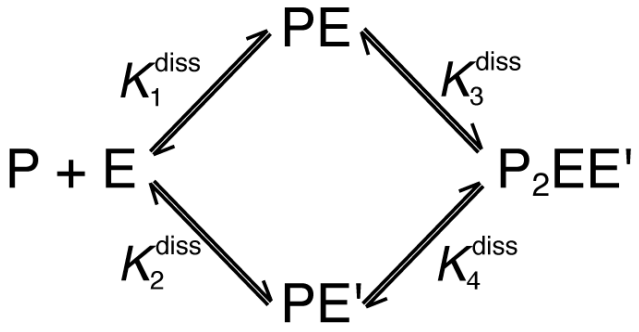

Scheme S1

It should be noted that in Scheme S1, $K_3^{\mathrm{diss}} = \alpha K_1^{\mathrm{diss}}$ and $K_4^{\mathrm{diss}} = \alpha K_2^{\mathrm{diss}}$ where α is the cooperativity factor (see main text).

The equilibrium concentrations of each of the species in Scheme S1 obey the following mass conservation relationships:

$$[\mathrm{E}]_\mathrm{T} = [\mathrm{E}] + [\mathrm{PE}] + [\mathrm{PE'}] + [\mathrm{P_2EE'}] \tag{S1}$$
$$[\mathrm{P}]_\mathrm{T} = [\mathrm{P}] + [\mathrm{PE}] + [\mathrm{PE'}] + 2[\mathrm{P_2EE'}] \tag{S2}$$

where $[\mathrm{P}]_\mathrm{T}$ and $[\mathrm{E}]_\mathrm{T}$ are the total concentrations of profilin and htt^{ex1}, respectively. By substituting the expressions for each dissociation constant K_j^{diss}, j = (1, 2, 3), into Eq. (S1), the following expression for the concentration of free htt^{ex1}, [E], is obtained,

$$[\mathrm{E}] = [\mathrm{E}]_\mathrm{T}\left\{1 + \frac{(K_1^{\mathrm{diss}} + K_2^{\mathrm{diss}})[\mathrm{P}]}{K_1^{\mathrm{diss}}K_2^{\mathrm{diss}}} + \frac{[\mathrm{P}]^2}{K_1^{\mathrm{diss}}K_3^{\mathrm{diss}}}\right\}^{-1} \tag{S3}$$

Substitution of Eq. (S3) into Eq. (S2) provides the following cubic equation,

$$a[\mathrm{P}]^3 + b[\mathrm{P}]^2 + c[\mathrm{P}] + d = 0 \tag{S4}$$

where $a = (K_1^{\mathrm{diss}}K_3^{\mathrm{diss}})^{-1}$, $b = (K_1^{\mathrm{diss}})^{-1} + (K_2^{\mathrm{diss}})^{-1} + (2[\mathrm{E}] - [\mathrm{P}]_\mathrm{T})(K_1^{\mathrm{diss}}K_3^{\mathrm{diss}})^{-1}$, $c = 1 + ([\mathrm{E}]_\mathrm{T} - [\mathrm{P}]_\mathrm{T})(1/K_1^{\mathrm{diss}} + 1/K_2^{\mathrm{diss}})$, and $d = -[\mathrm{P}]_\mathrm{T}$. Numerical solution of Eq. (S4) for [P] - a function $f(K_j^{\mathrm{diss}}; [\mathrm{E}]_\mathrm{T}; [\mathrm{P}]_\mathrm{T})$ - which we denote by 'S' in the following, can be used in conjunction with Eq. (S3) and the expressions for each constant K_j^{diss}, to obtain the expressions for equilibrium concentrations of complex i, $i \in$ {**PE**, **PE′**, **P$_2$EE′**},

$$[\mathrm{PE}] = S\lambda[\mathrm{E}]_\mathrm{T}/K_1^{\mathrm{diss}} \tag{S5.1}$$

$$[\mathrm{PE'}] = S\lambda[\mathrm{E}]_\mathrm{T}/K_2^{\mathrm{diss}} \tag{S5.2}$$

$$[\mathrm{P_2EE'}] = S^2\lambda[\mathrm{E}]_\mathrm{T}/(K_1^{\mathrm{diss}}K_3^{\mathrm{diss}}) \tag{S5.3}$$

where

$$\lambda = \left\{1 + \frac{(K_1^{\mathrm{diss}} + K_2^{\mathrm{diss}})S}{K_1^{\mathrm{diss}}K_2^{\mathrm{diss}}} + \frac{S^2}{K_1^{\mathrm{diss}}K_3^{\mathrm{diss}}}\right\}^{-1} \tag{S5.4}$$

The real solution 'S' of Eq. (S4) for [P] can also be obtained analytically and has the form,

$$S = 9a^2L^3 - 3abL^2 - 3ac - b^2 \tag{S6}$$

where

$$L=\left\{\frac{9a\sqrt{(4/3)ac^3-(1/3)b^2c^2+6abc[P]_T-(4/3)b^3[P]_T+9a^2[P]_T^2}+27a^2[P]_T+9abc-2b^3}{54a^3}\right\}^{1/3} \tag{S7}$$

The fractional population p_i of the complex i, $i \in \{\mathbf{PE}, \mathbf{PE'}, \mathbf{P_2EE'}\}$, can then be obtained by division of each equilibrium concentration in Eqs. (S5.1-5.3) by the total concentration of the observable species ($[E]_T$ or $[P]_T$). Note that fractional populations p_i are defined differently for the two types of titrations: when ^{15}N-labeled profilin is titrated with unlabeled htt^{ex1}, the total concentration of observable species is $[P]_T$, whereas when ^{15}N-labeled htt^{ex1} is titrated with unlabeled profilin, the corresponding total concentration is $[E]_T$. The fourth dissociation constant, K_4^{diss} (Scheme S1) is calculated *a-posteriori*, $K_4^{diss} = K_1^{diss}K_3^{diss}/K_2^{diss}$.

The measured values of ^{15}N-δ_{ex} and ^{15}N-ΔR_2 for ^{15}N-labeled htt^{ex1} in the presence of profilin, and the ^{15}N-δ_{ex} values measured for ^{15}N-labeled profilin in the presence of unlabeled htt^{ex1}, were fit simultaneously by minimizing the following target function (F),

$$\begin{aligned}F=\alpha_1\sum_i\left(\frac{\delta_{ex,P11}^{obs,i}-\delta_{ex,P11}^{calc,i}}{\sigma_{\delta_{ex,P11}}^{i}}\right)^2+\alpha_2\sum_j\left(\frac{\delta_{ex,P10}^{obs,j}-\delta_{ex,P10}^{calc,j}}{\sigma_{\delta_{ex,P10}}^{j}}\right)^2+\alpha_3\sum_k\left(\frac{\Delta R_{2,P11}^{obs,k}-\Delta R_{2,P11}^{calc,k}}{\sigma_{\Delta R_{2,P11}}^{k}}\right)^2+\\ \alpha_4\sum_l\left(\frac{\Delta R_{2,P10}^{obs,l}-\Delta R_{2,P10}^{calc,l}}{\sigma_{\Delta R_{2,P10}}^{l}}\right)^2+\alpha_5\sum_m\left(\frac{\delta_{ex,Prof}^{obs,m}-\delta_{ex,Prof}^{calc,m}}{\sigma_{\delta_{ex,Prof}}^{m}}\right)^2\end{aligned} \tag{S8}$$

where the first two terms correspond to the differences between the observed ('obs') and calculated ('calc') ^{15}N-δ_{ex} values measured for the two pairs of htt^{ex1} residues - [Gln22; Gln23] and [Gly62; Val65] - that describe the binding of profilin to the polyproline P_{11} and P_{10} tracts, respectively; the third and the fourth terms correspond to the ^{15}N-ΔR_2 data measured for the same two pairs of htt^{ex1} residues; the last term corresponds to the ^{15}N-δ_{ex} values measured for ^{15}N-labeled profilin ('Prof') in the presence of unlabeled htt^{ex1}; and 'σ' denotes experimental errors. The subscripts i, j, k, l and m refer to residue numbers for each set of data ($i = 2$, $j = 2$, $k = 2$, $l = 2$, $m = 4$). The coefficients $\alpha_{1\text{-}5}$ are empirically determined weighting factors for different types of data: $\alpha_1 = \alpha_3 = \alpha_4 = \alpha_5 = 1$, and $\alpha_2 = 0.5$. The set of global variable parameters in the minimization of the target function comprised, K_j^{diss}, $j = 1, 2, 3$, while the space of local (residue-specific) variable parameters included: (i) the differences between the chemical shifts of the complexes and the monomeric species, $\Delta\omega$, for each residue of profilin or htt^{ex1} (assumed the same for the single-occupied, **PE** and **PE′**, and double-occupied, **P₂EE′**, species in Scheme S1, as described in the main text); (ii) transverse ^{15}N spin relaxation rates R_2 for the single-occupied species **PE** or **PE′** (assumed equal), $R_{2,PE} = R_{2,PE'}$. The relaxation rates of the doubly-occupied species **P₂EE′** were scaled according to the ratio of molecular weights of the double-occupied (38 kDa) and singly-occupied htt^{ex1} (23 kDa), and equal to $1.65R_{2,PE}$. The fast exchange limit was assumed for lifetime line broadening, ΔR_2, where $\Delta R_2 = p_i(R_{2,i} - R_2)$, $i \in \{\mathbf{PE}, \mathbf{PE'}, \mathbf{P_2EE'}\}$, and R_2 is the relaxation rate of free htt^{ex1}. The best-fit populations p_i, $i \in \{\mathbf{PE}, \mathbf{PE'}, \mathbf{P_2EE'}\}$, for ^{15}N-

labeled htt^{ex1} titrated with unlabeled profilin, and ^{15}N-labeled profilin titrated with unlabeled htt^{ex1}, are shown in Fig. 4D of the main text.

Analysis of the binding kinetics of profilin-htt^{NT}Q$_7$P$_{11}$K$_2$ interactions. The ^{15}N-δ_{ex} titration curves and proline^{13}Cα-CPMG relaxation dispersion profiles obtained for htt^{NT}Q$_7$P$_{11}$K$_2$ in the presence of unlabeled profilin, and ^{15}N-δ_{ex} titration curves, ^{15}N-CPMG relaxation dispersion profiles and ^{15}N-δ_{ex} data obtained for profilin in the presence of unlabeled htt^{NT}Q$_7$P$_{11}$K$_2$, were best-fit simultaneously to the kinetic model shown in Scheme S2 and Figure 5F of the main text:

$$E_S + P \underset{k_{off}}{\overset{k_{on}}{\rightleftharpoons}} E_SP$$

Scheme S2

where the bimolecular (second order) nature of profilin(P)-htt^{NT}Q$_7$P$_{11}$K$_2$(E$_S$) complex formation is considered explicitly. Such a treatment is advantageous in the case of profilin-htt^{NT}Q$_7$P$_{11}$K$_2$ interactions, as the kinetics of complex formation can be monitored from the perspective of each of the binding partners, whose total concentrations are known with sufficient accuracy. The calculations of CPMG relaxation dispersion profiles and exchange induced shifts (δ_{ex}) were performed as described previously (2). The second-order association rate-constant k_{on} and the dissociation rate constant k_{off} were the two global variable parameters of the fit. The pseudo-first-order, 'apparent' association rate constant, k_{on}^{app}, that enters into the exchange matrix, was re-cast as, $k_{on}^{app} = k_1[B_i]$, $i \in \{P; E_S\}$, and $[B_i]$ denotes the equilibrium concentration of (free) species i (P or E$_S$ depending on which binding partner is observed). At each step (iteration) of the minimization, the concentration of B_i, $i \in \{P, E_S\}$, is given by, $[B_i] = [B_i]_T - p_B^j[B_j]_T$, where $[B_i]_T$ and $[B_j]_T$ are the total concentrations of the two binding partners, $i, j \in \{P; E_S\}$, $i \neq j$, and the population of the bound state j, p_B^j, is calculated from the solution of the quadratic equation obtained from the material balance,

$$p_B^j = \left\{ \left([B_i]_T + [B_j]_T + K^{diss} \right) - \left(\left\{ [B_i]_T + [B_j]_T + K^{diss} \right\}^2 - 4[B_i]_T[B_j]_T \right)^{\frac{1}{2}} \right\} \left(2[B_j]_T \right)^{-1} \quad \text{(S9)}$$

where $K^{diss} = k_{off}/k_{on}$; $i, j \in \{P; E_S\}$, and $i \neq j$.

The array of local (residue-specific) variable parameters comprised, $\left\{ \Delta\omega_{E_S}^{N,i}, \Delta\omega_{E_S}^{CA,j}, \Delta\omega_P^{N,k}, \Delta\omega_P^{H,m}, R_{2,E_S}^{CA,600,j}, R_{2,E_S}^{CA,800,j}, R_{2,P}^{N,600,l}, R_{2,P}^{N,800,l} \right\}$, where $\Delta\omega$ denotes the differences between the chemical shifts of the bound species (E$_S$P) and those of the free htt^{NT}Q$_7$P$_{11}$K$_2$ ('E$_S$') or profilin ('P'); R_2 is the transverse spin relaxation rate of the free species (E$_S$ or P). The superscripts denote the type of the nucleus ('N' ≡ '^{15}N'; 'CA' ≡ '^{13}Cα'; 'H' ≡ '^{1}H$_N$'), ^{1}H spectrometer frequency (600 and 800 MHz), and the number of residues analyzed (i = 4, j = 2, k = 8, l = 5, and m = 1).

Analysis of ^{15}N-CPMG relaxation dispersion data obtained for htt^{ex1} in the presence of unlabeled profilin. ^{15}N-CPMG relaxation dispersion data were obtained for htt^{ex1} in the presence of saturating amounts of profilin that hinders the formation of the on-pathway dimeric and tetrameric species (the pathways shown in grey in Fig. 6C, main text). The relaxation dispersion profiles were collected at two concentrations of htt^{ex1} (0.40 and 0.75 mM), and the dataset consisting of the 11 htt^{ex1} residues (Fig. 6B,

main text, and Fig. S12) that do not show chemical shift changes upon addition of profilin was best-fit globally to a two-state model of exchange, shown in black in Fig. 6C of the main text. The calculation of CPMG relaxation dispersion profiles was performed by solution of a set of Bloch-McConnell equations as described previously (2, 16).The second-order self-association rate constant k_3^* and the dissociation rate constant k_{-3}^*were used as the global variable parameters in the fit. The 'apparent' pseudo-first-order self-association rate constant that enters into the exchange matrix, is given by, $k_3^{\mathrm{app},*} = 2k_3^*[\mathbf{EP}]$, where [**EP**] is the concentration of the profilin-htt^{ex1} complex **EP** (94.3 % of the total htt^{ex1} concentration under the conditions of our study; see main text). The array of local (residue-specific) parameters varied in the fit comprised: $\left\{\Delta\omega^{\mathrm{N}}; R_2^{\mathrm{N},600,C_1}, R_2^{\mathrm{N},800,C_1}, R_2^{\mathrm{N},600,C_2}, R_2^{\mathrm{N},800,C_2}\right\}$, where $\Delta\omega^{\mathrm{N}}$ is the difference between ^{15}N chemical shifts of profilin-bound htt^{ex1} in the dimeric state $(\mathbf{EP})_2^*$ and the Profilin-bound htt^{ex1} monomer (**EP**); R_2 is ^{15}N transverse spin relaxation rate of the state **EP** (R_2 of the bound dimeric species $(\mathbf{EP})_2^*$ was assumed to be equal to $2R_{2,\mathrm{EP}}$); and the superscripts denote the type of nucleus ('N' ≡ '^{15}N'), spectrometer field (600 and 800 MHz), and the two concentrations C_n of htt^{ex1} at which the data were collected (C_1 = 0.40 mM and C_2 = 0.75 mM).

Minimization. Minimization of all error functions was performed using the 'trust-region-reflective' algorithm for constrained non-linear minimization in an in-house program implemented in Matlab (MathWorks Inc., MA). In all the calculations the uncertainties in the fitted values of the optimized parameters, corresponding to ± 1 S.D., were determined from the Jacobian variance-covariance matrix of the nonlinear fit. Uncertainties in parameters derived from the optimized parameters (e.g. K_{diss} from the ratio of the optimized values of k_{off} and k_{on}) were determined by standard propagation of errors.

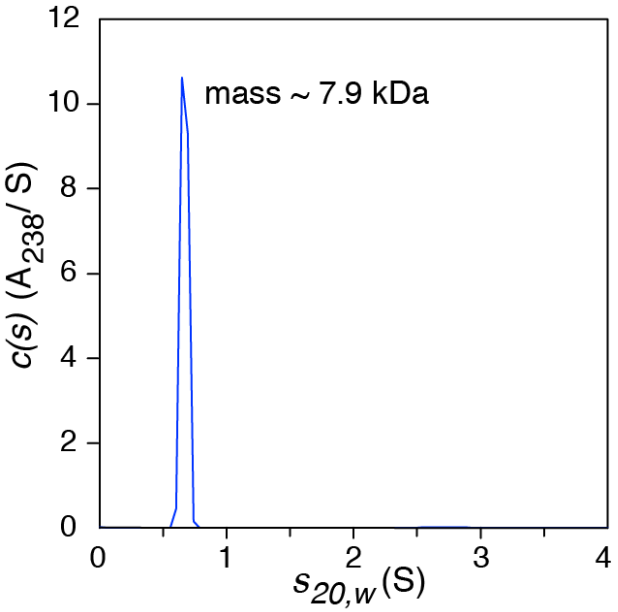

Figure S1. Characterization of htt^{ex1} by sedimentation velocity analytical ultracentrifugation. The sedimentation velocity absorbance profile, *c(s)*, was obtained for 1.2 mM htt^{ex1}. Only a single species at 0.74 S with an estimated molecular mass of 7.9 kDa is observed, indicating that the observable species is monomeric. The data were collected at 10 °C in 20 mM sodium phosphate buffer, pH 6.5, 50 mM NaCl and 90% H_2O/10 % D_2O (v/v).

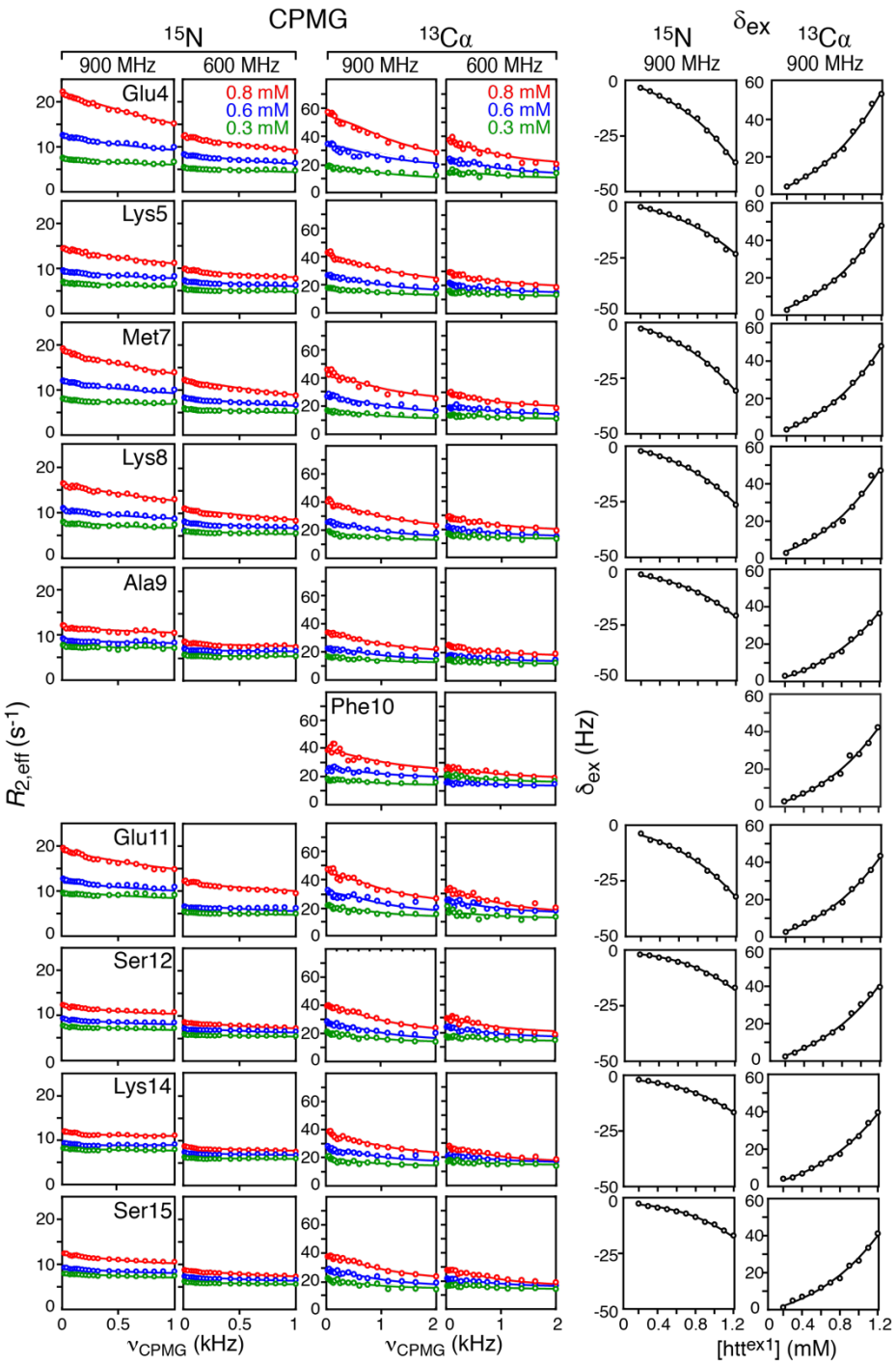

Figure S2. Concentration dependent ^{15}N and ^{13}Cα CPMG relaxation dispersion profiles, and ^{15}N and ^{13}Cα exchange induced shifts (δ_{ex}) used for quantitative analysis of pre-nucleation oligomerization of ^{15}N/^{13}Cα-labeled htt^{ex1}. The data were recorded at 5 °C. The experimental points are shown as circles, and the best fit curves to the branched kinetic scheme shown in Fig. 2D of the main text are shown as continuous lines. Details of the fitting procedure are provided in the *Appendix SI*. Note that the ^{15}N data for Phe10 were not included in the global fit as the ^{15}N-CPMG dispersion profiles and concentration-dependent changes in ^{15}N-δ_{ex} are very small. The reduced χ^2 is 2.25, calculated with errors of 0.3 Hz and 0.6 s^{-1} for the δ_{ex} and CPMG relaxation dispersion data, respectively.

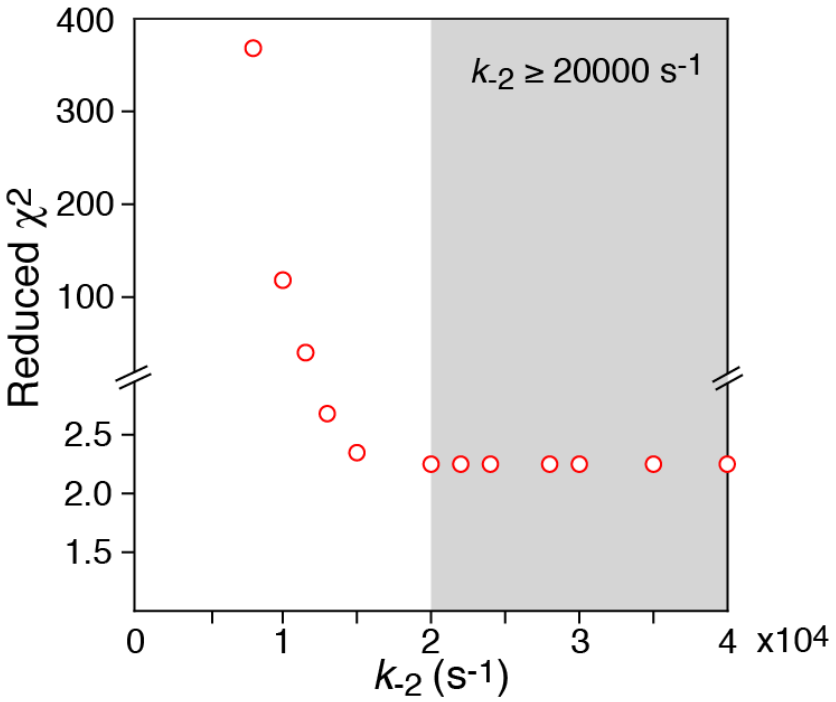

Figure S3. Grid search showing the dependence of the reduced χ^2 on the value of k_{-2}, the dissociation rate constant of the tetramer into two on-pathway ('productive') dimers. k_2 and k_{-2} are linearly correlated: thus, the equilibrium dissociation constant K_2^{diss} can be determined, and the χ^2 grid search indicates that the lower limit of k_{-2} consistent with the δ_{ex} and CPMG relaxation dispersion data is ~20,000 s^{-1}. The overall dissociation rate constant from tetramer to monomer is given by $k_{-1}k_{-2}/(k_{-1}+ k_2^{app}) = k_{-1}^2k_{-2}/(k_{-1}^2 + 2k_1k_2[\mathbf{E}]^2)$, and therefore decreases as the concentration of monomer increases, thereby affecting the overall rate of interconversion (k_{ex}) between monomer and tetramer (2).

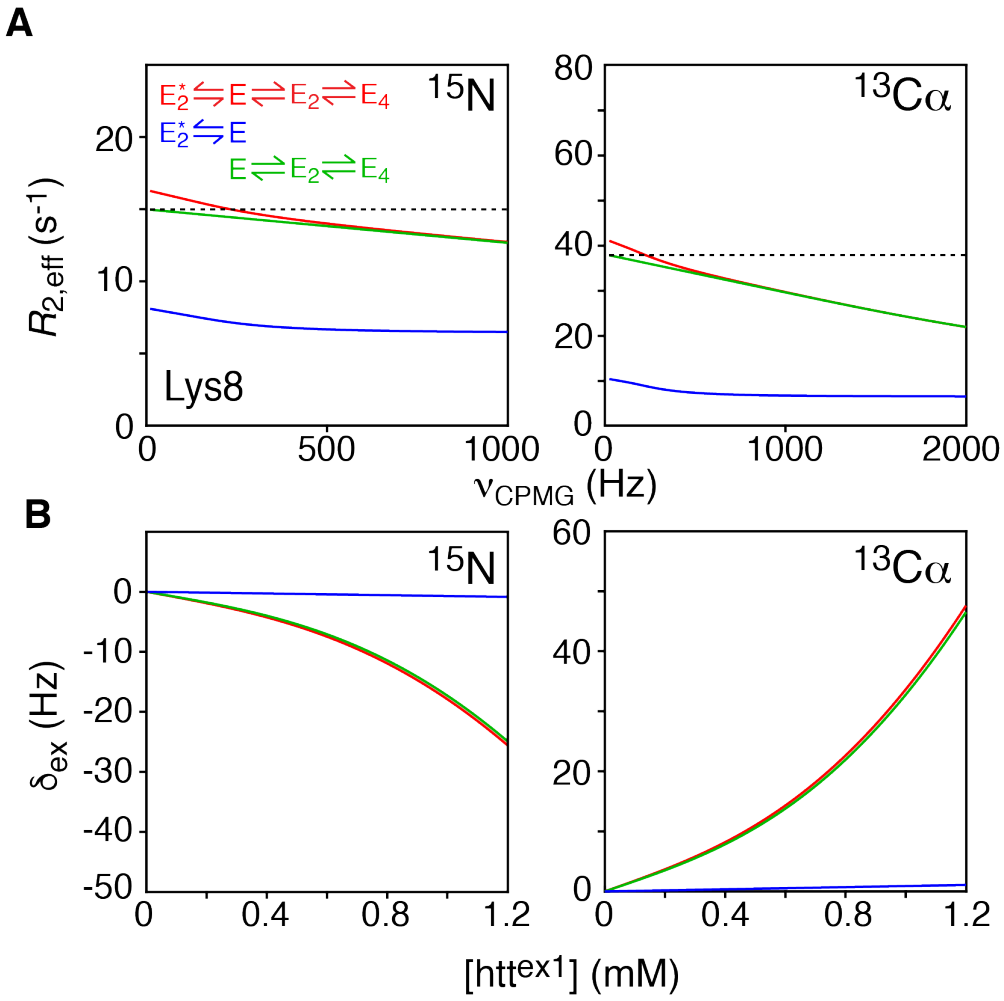

Figure S4. Simulation illustrating the contribution of the 'productive' and 'non-productive' pathways for htt^{ex1} oligomerization to the ^{15}N and ^{13}Cα CPMG relaxation dispersion profiles and concentration-dependent exchange-induced (δ_{ex}) shifts. Simulated curves for the full branched four-state exchanging system, the 'non-productive' dimerization pathway and the 'productive' pathway leading to a tetramer are displayed in red, blue and green, respectively. (A) ^{15}N and ^{13}Cα CPMG profiles and (B) ^{15}N- and ^{13}Cα exchange-induced shifts at 900 MHz. The total htt^{ex1} concentration in panel A is 0.8 mM; the values of the rate constants used in the simulations, obtained from the global fits to the full four-state kinetic scheme (shown in red in panel A, as well as in Fig. 2D) to the NMR data shown in Fig. S2 (and Fig. 2, main text), are as follows: k_1= 5.8 x 10^5 M^{-1}s^{-1}, k_{-1} = 4.1 x 10^4 s^{-1}, k_2 = 8.5 x 10^8 M^{-1}s^{-1}, k_{-2} = 2.0 x 10^4 s^{-1}, k_3 = 5.9 x 10^3 M^{-1}s^{-1} and k_{-3}= 1350 s^{-1}; ^{15}N and ^{13}Cα R_2 (monomer) = 6.4 and 11.7 s^{-1} and with R_2(dimer) = 2 x R_2(monomer) and R_2(tetramer) = 4 x R_2(monomer). The values of Δω for the different species used in the simulation correspond to those for Lys8 listed in Table S1.

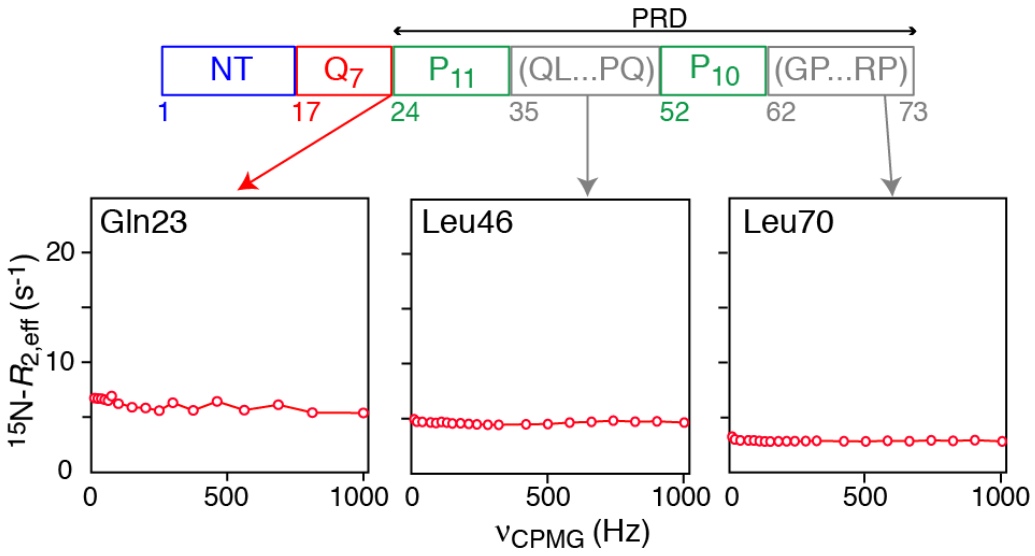

Figure S5. Examples of ^{15}N-CPMG relaxation dispersion profiles observed for 0.8 mM ^{15}N/^{13}Cα-labeled htt^{ex1} at the C-terminal end of the polyglutamine (Q_7) region (Gln23), in the linker (Leu46) connecting the two polyproline tracts (P_{11} and P_{10}), and close to the C-terminus (Leu70). No significant ^{15}N-CPMG dispersions (^{15}N-R_{ex} > 2 s^{-1}) are observed beyond Gln17. The experimental data were recorded at 5 °C.

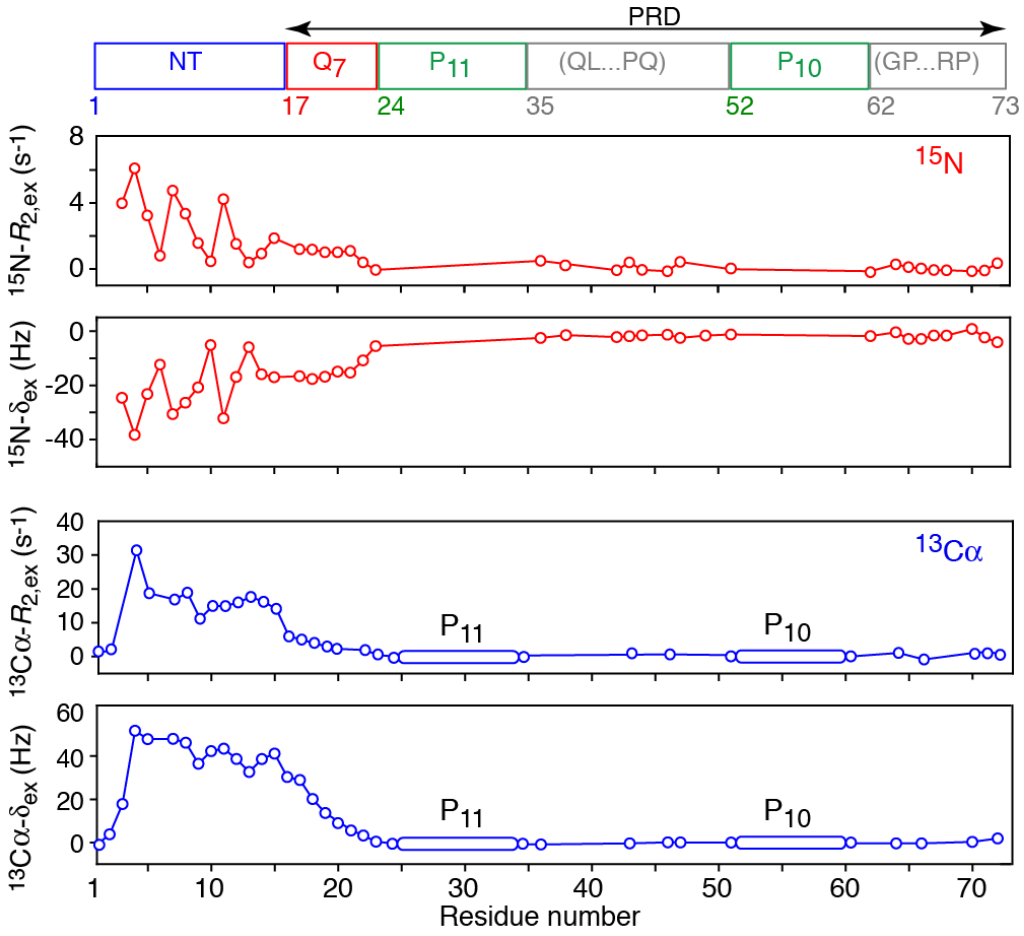

Figure S6. Profiles of ^{15}N and ^{13}Cα exchange contributions to transverse relaxation ($R_{2,ex}$) and exchange induced shifts (δ_{ex}) for htt^{ex1}. The domain architecture of htt^{ex1} is shown at the top of the figure. The R_{2ex} values were obtained from ^{15}N- and ^{13}Cα CPMG relaxation dispersion experiments recorded on a 0.8 mM ^{15}N/^{13}Cα-labeled htt^{ex1} sample. The δ_{ex} values were obtained by taking the differences in ^{15}N and ^{13}Cα chemical shifts (obtained from ^{1}H-^{15}N and ^{1}H-^{13}C HSQC experiments, respectively) between 1.2 mM and 50 μM samples of ^{15}N/^{13}C-labeled htt^{ex1}. The ^{13}Cα-δ_{ex} and $R_{2,ex}$ values obtained for the overlapped ^{1}Hα-^{13}Cα proline cross-peaks of Pro25 to Pro33 and Pro53 to Pro60, are shown with ovals covering the P_{11} and P_{10} polyproline tracts, respectively. All data were recorded at 5 °C and 900 MHz.

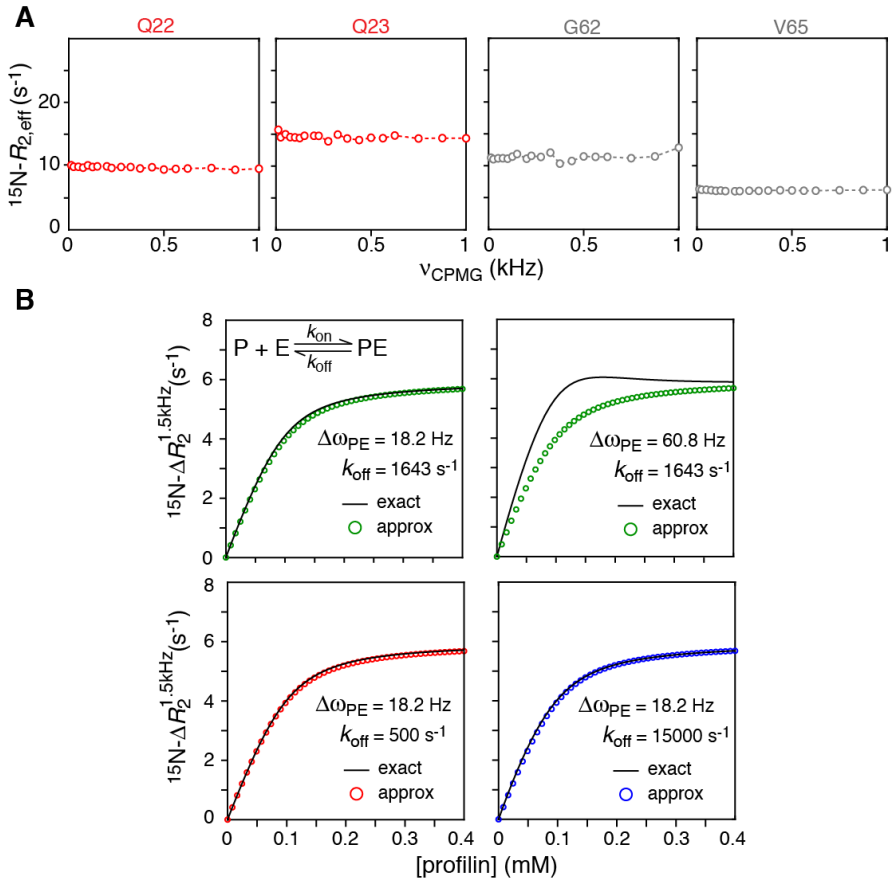

Figure S7. Exchange regime with respect to ^{15}N-$\Delta R_2^{1.5\ kHz}$ lifetime line broadening for the binding of profilin to htt^{ex1}. (A) No ^{15}N-CPMG dispersions are observed for Gln22/Gln23 and Gly62/Val65 under conditions where ^{15}N-exchange induced shifts and ^{15}N-$\Delta R_2^{1.5\ kHz}$ lifetime line broadening are observed for these residues (see Fig. 4B, main text). The data were recorded at 5 °C and 600 MHz; the concentrations of ^{15}N-labeled htt^{ex1} and unlabeled profilin are 400 μM each. (B) Simulations showing a comparison of the exact concentration dependence of ^{15}N-$\Delta R_2^{1.5\ kHz}$ lifetime line broadening (solid lines) calculated from the Bloch-McConnell equations with that calculated for the fast-exchange approximation (circles). The bottom left, top left and bottom right panels show the results for k_{off} = 500, 1643 and 15,000 s^{-1}, respectively, for $\Delta\omega_{PE}$ = 18.2 Hz (0.3 ppm at 600 MHz) which is slightly larger than the largest value observed experimentally for ^{15}N-δ_{ex} (Fig. 4B, main text). The concentration of htt^{ex1}, E, is 100 μM; k_{on} = 3.2 x 10^7 M^{-1}s^{-1}. The values of k_{off} = 1643 s^{-1} and k_{on} = 3.2 x 10^7 M^{-1}s^{-1} correspond to those obtained experimentally for the binding of profilin to the shorter htt^{NT}Q$_7$P$_{11}$K$_2$ construct (see Fig. 5, main text). When $\Delta\omega_{PE}$ is increased to 60.8 Hz (top right panel; 1 ppm at 600 MHz), significant deviations are observed between the exact solution and the fast exchange approximation.

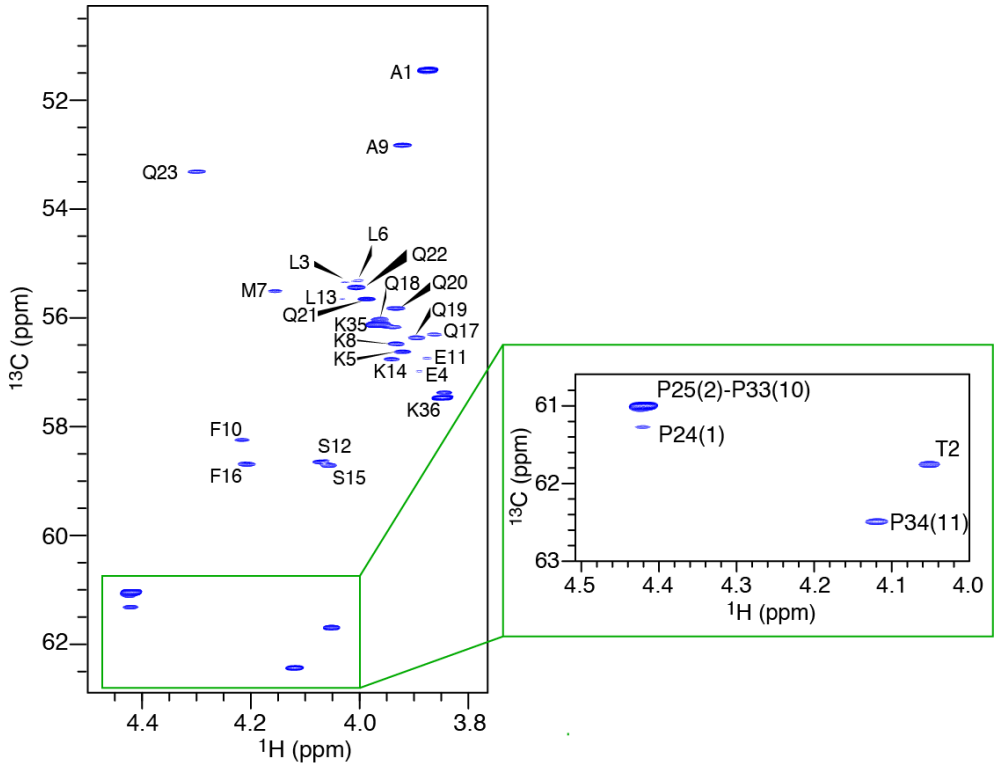

Figure S8. 2D ^{1}H-^{13}C constant-time HSQC spectrum of 1.0 mM sample of ^{15}N/^{13}Cα-labeled htt^{NT}Q$_7$P$_{11}$K$_2$ (5 °C, 600 MHz) in 20 mM phosphate buffer, pH 6.5, 50 mM NaCl and 90% H_2O/10 % D_2O (v/v). The region of the proline ^{1}Hα/^{13}Cα cross-peaks is enclosed in the green box and enlarged on the right-hand side of the figure.

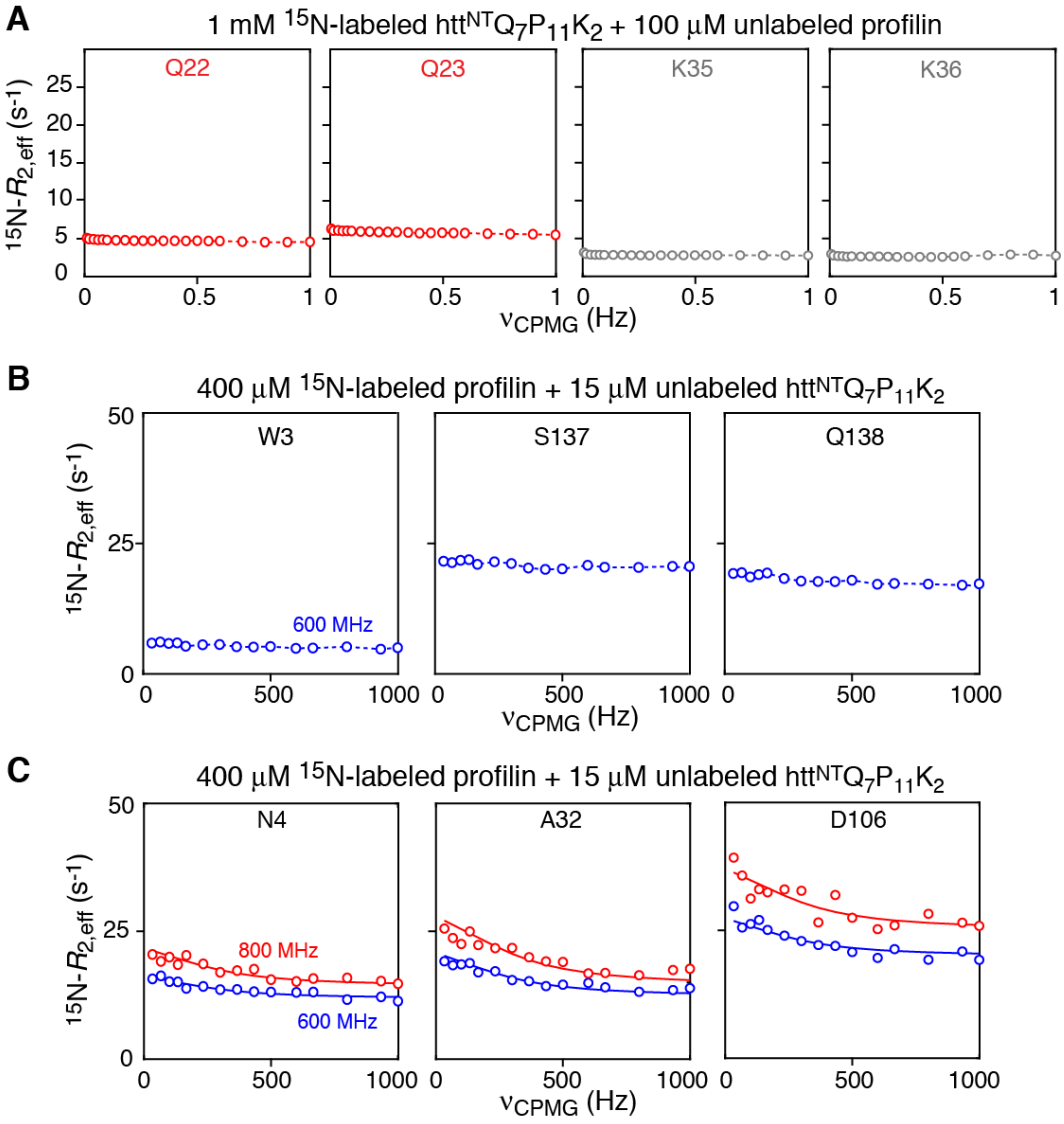

Figure S9. Additional ^{15}N-CPMG relaxation dispersion profiles used in data analysis of the binding kinetics of profilin-htt^{NT}Q$_7$P$_{11}$K$_2$ interaction. (A) ^{15}N/^{13}Cα-labeled htt^{NT}Q$_7$P$_{11}$K$_2$ in the presence of unlabeled profilin. (B) and (C) ^{15}N/^{13}C-labeled profilin in the presence of unlabeled htt^{NT}Q$_7$P$_{11}$K$_2$. The circles represent the experimental data. Since no or minimal dispersions are observed in panels A and B, the dashed lines serve purely to guide the eye. The solid lines in panel C are the best-fit curves obtained from global fitting to the two-state kinetic scheme shown in Scheme S2 and Fig. 5F (main text). All experimental data were recorded at 5 °C.

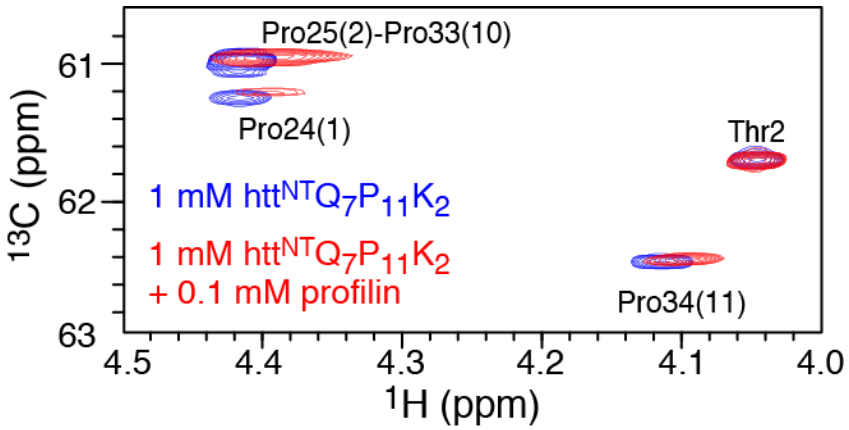

Figure S10. Addition of profilin to $^{15}N/^{13}C\alpha$-labeled $htt^{NT}Q_7P_{11}K_2$ results in negative shifts of the proline $^{1}H\alpha$ and $^{13}C\alpha$ resonances in the P_{11} polyproline tract. The blue and red contours are the spectra obtained in the absence and presence of profilin, respectively. The 2D ^{1}H-^{13}C constant-time HSQC spectra were recorded at 5 °C and 600 MHz in 20 mM phosphate buffer, pH 6.5, 50 mM NaCl and 90% H_2O/10 % D_2O (v/v). Note that further addition of profilin results in extensive line broadening and disappearance of the $^{1}H\alpha/^{13}C\alpha$ proline cross-peaks.

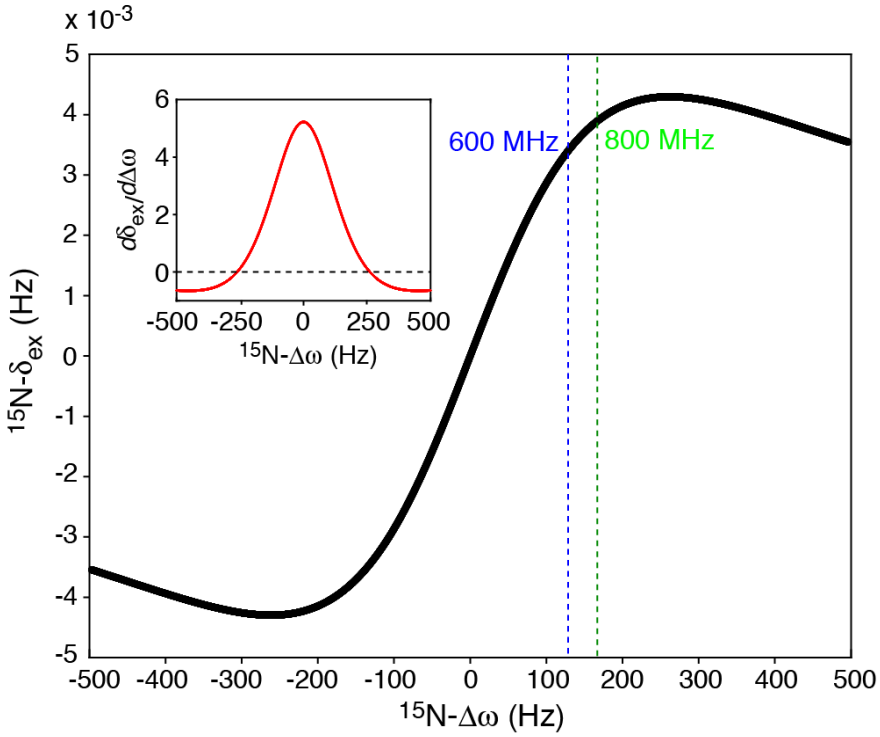

Figure S11. Simulation of ^{15}N exchange-induced chemical shift (^{15}N-δ_{ex}) as a function of the difference ($\Delta\omega$) between the chemical shifts of profilin bound to htt^{NT}Q$_7$P$_{11}$K$_2$ (ω_B) and free profilin (ω_A): $\Delta\omega_{AB} = \omega_B - \omega_A$. The curve is calculated from the imaginary part of the smallest (by absolute magnitude) eigenvalue of the evolution Liouvillian (Eq. S1 in *SI Appendix* of Ref. 2). The following average parameters of exchange for profilin binding to htt^{NT}Q$_7$P$_{11}$K$_2$ were used in the simulation (see Fig. 5F of main text): k_{on}^{app}= 54 s^{-1}, k_{off} = 1643 s^{-1} (corresponding to a population of 3.2% for the complex), and $R_{2,A} = R_{2,B}$ = 18 s^{-1}. The average ^{15}N-$\Delta\omega$ values of 2.1 ppm obtained for profilin at 600 MHz (equivalent to 128 Hz) and 800 MHz (equivalent to 170 Hz) are indicated by the blue and green dashed vertical lines, respectively. The derivative of the function $\delta_{ex}(\Delta\omega)$, $d\delta_{ex}/d\Delta\omega$, is shown in the inset, where the horizontal dashed line is drawn at the value of $d\delta_{ex}/d\Delta\omega = 0$. It is clear from the plot that for the average values of $\Delta\omega$ obtained from the global fit (and, generally, for $|^{15}\text{N-}\Delta\omega| \geq 2$ ppm in the case of profilin-htt^{NT}Q$_7$P$_{11}$K$_2$ interactions), a very weak field dependence of ^{15}N-δ_{ex} values is predicted - in agreement with barely distinguishable values of ^{15}N-δ_{ex} obtained experimentally at 600 and 800 MHz in Fig. 5E (main text).

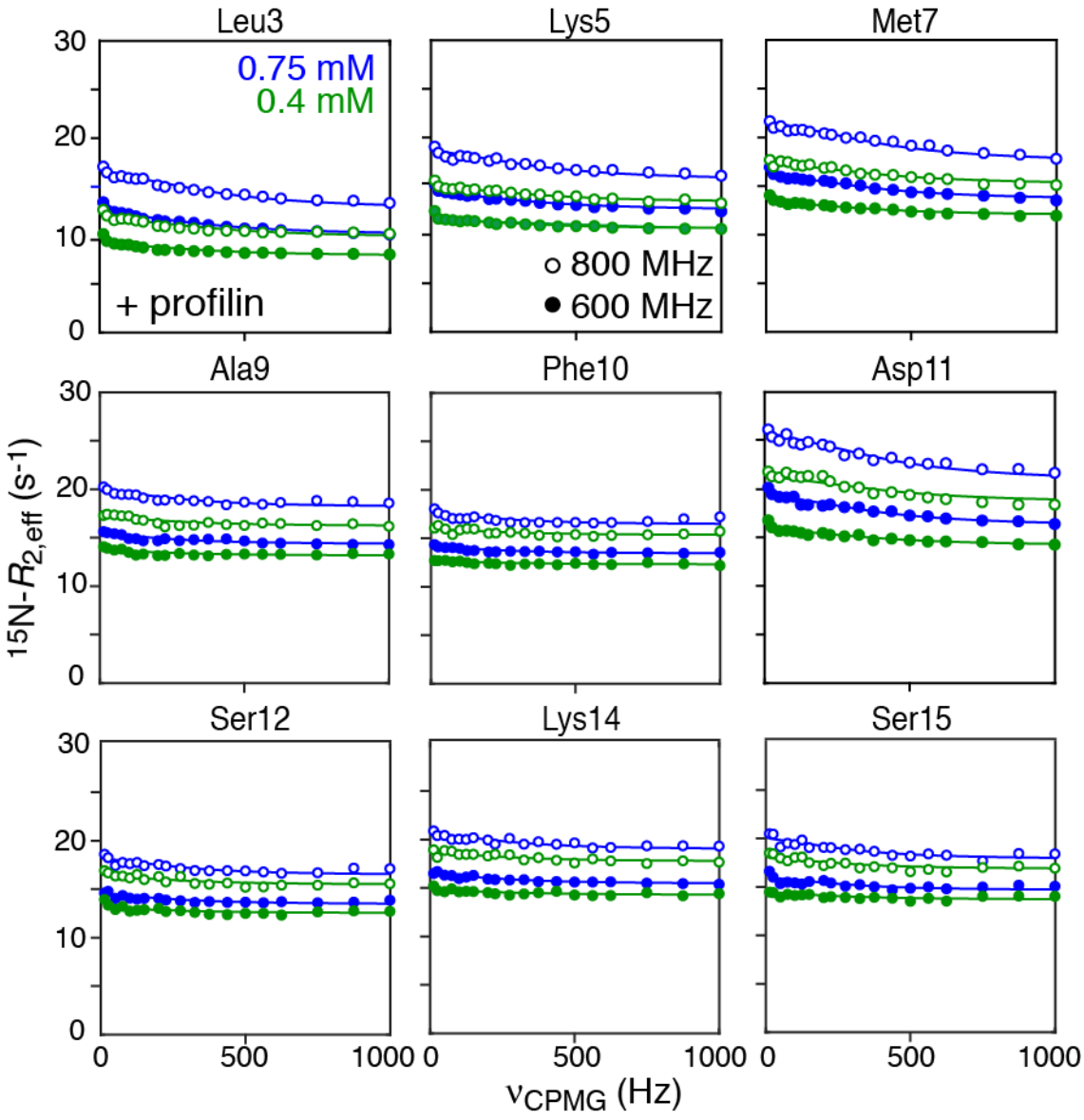

Figure S12. Additional ^{15}N-CPMG relaxation dispersion profiles for 0.4 and 0.75 mM ^{15}N/^{13}Cα-labeled htt^{ex1} in the presence of 4.8 mM unlabeled profilin. The data were recorded at 5 °C. The filled-in and open circles represent data acquired at 600 and 800 MHz, respectively. The solid lines represent the best-fit curves obtained from the global fit to the two-state kinetic scheme shown in Fig. 6C (main text). For errors of 0.3 s^{-1} for the ^{15}N CPMG relaxation dispersion data, the reduced χ^2 is 0.77.

Table S1. Residue-specific fitted values of Δω (ppm) for the 'non-productive' dimer ($\mathbf{E_2^*}$) and 'productive' dimer/tetramer ($\mathbf{E_2}$, $\mathbf{E_4}$) obtained from the global fits to the relaxation dispersion and exchange-induced shift data for free htt^{ex1}.[a]

	Off-pathway $\Delta\omega_{E_2^*}$ (ppm)		On-pathway $\Delta\omega_{E_2,E_4}$ (ppm)	
Residue	^{15}N	^{13}Cα	^{15}N	^{13}Cα [a]
4	-1.25 ± 0.20	1.51 ± 0.13	-5.02 ± 0.96	3.26 ± 0.69
5	-1.13 ± 0.19	0.91 ± 0.10	-3.06 ± 0.56	2.72 ± 0.54
7	-1.34 ± 0.19	1.10 ± 0.10	-3.96 ± 0.74	2.65 ± 0.53
8	-1.15 ± 0.19	0.87 ± 0.09	-3.33 ± 0.62	2.67 ± 0.52
9	-0.59 ± 0.31	0.88 ± 0.09	-2.60 ± 0.48	1.99 ± 0.38
10	-	1.01 ± 0.09	-	2.30 ± 0.45
11	-1.06 ± 0.21	2.74 ± 0.19	-3.95 ± 0.74	2.36 ± 0.46
12	-0.84 ± 0.22	1.84 ± 0.14	-2.08 ± 0.38	2.22 ± 0.43
14	-0.67 ± 0.26	1.20 ± 0.10	-1.94 ± 0.36	2.08 ± 0.40
15	-1.03 ± 0.19	1.35 ± 0.11	-1.90 ± 0.34	2.23 ± 0.43

[a] ^{13}Cα and ^{15}N Δω values of the productive dimer ($\mathbf{E_2}$) and tetramer ($\mathbf{E_4}$) are assumed to be the same. To ensure a stable solution during minimization, the ^{13}Cα Δω values of the off-pathway dimer ($\mathbf{E_2^*}$) were constrained to be positive, while those of the on-pathway dimer ($\mathbf{E_2}$) and tetramer ($\mathbf{E_4}$) (assumed to be the same) were constrained within a range of ±0.5 ppm from the values reported previously for the smaller htt^{NT}Q$_7$ construct (2): specifically, 2.86, 2.56, 2.30, 2.32 1.91, 2.33, 2.25, 2.32, 2.12 and 2.60 ppm for residues 4, 7, 5, 8, 9 10, 11, 12, 14 and 15 respectively. The ^{13}Cα Δω values listed in the Table all fall well within these ranges.

Table S2. Residue-specific fitted values of ^{15}N/^{1}H-Δω and ^{15}N-R_2 (for htt^{ex1} only) obtained from the global fit to the concentration-dependence of the ^{15}N-δ_{ex} data for ^{15}N-labeled profilin titrated with unlabeled htt^{ex1} and the concentration-dependence of the ^{15}N-δ_{ex} and ^{15}N-ΔR_2 data for ^{15}N-labeled htt^{ex1} titrated with unlabeled profilin.

Profilin

Residue	^{15}N-$\Delta\omega_{PE,PE',P_2EE'}$(ppm)
3	0.10 ± 0.06
137	0.30 ± 0.08
138	0.68 ± 0.14

Residue	^{1}H-$\Delta\omega_{PE,PE',P_2EE'}$(ppm)
3	0.26 ± 0.08

htt^{ex1}

Residue	^{15}N-$\Delta\omega_{PE,P_2EE'}$(ppm)	^{15}N-$R_{2,PE}$(s^{-1})
22	0.17 ± 0.02	11.0 ± 0.6
23	0.30 ± 0.03	11.8 ± 0.6

Residue	^{15}N-$\Delta\omega_{PE',P_2EE'}$(ppm)	^{15}N-$R_{2,PE'}$(s^{-1})
62	0.15 ± 0.01	13.6 ± 1.3
65	0.13 ± 0.01	11.0 ± 1.1

Table S3. Residue-specific fitted values of $^{15}N/^{1}H$-Δω and ^{15}N-R_2 obtained for ^{15}N-labeled profilin in the presence of unlabeled $htt^{NT}Q_7P_{11}K_2$, and for ^{15}N-Δω, $^{13}C\alpha$-Δω and $^{13}C\alpha$-R_2 obtained for $^{15}N/^{13}C\alpha$-labeled $htt^{NT}Q_7P_{11}K_2$ in the presence of unlabeled profilin.

Profilin

Residue	^{15}N-$\Delta\omega_{E_SP}$(ppm)	Residue	^{15}N-$\Delta\omega_{E_SP}$(ppm)	^{15}N-R_{2,E_SP}^{600MHz}(s^{-1})	^{15}N-R_{2,E_SP}^{800MHz}(s^{-1})
3	0.09 ± 0.01	4	1.25 ± 0.06	12.3 ± 1.2	14.7 ± 1.5
137	0.19 ± 0.02	5	2.80 ± 0.10	18.5 ± 1.5	22.3 ± 2.1
138	0.61 ± 0.02	7	2.30 ± 0.09	15.9 ± 1.4	22.9 ± 1.8
		32	1.62 ± 0.08	13.3 ± 1.3	16.0 ± 1.6
	^{1}H-$\Delta\omega_{E_SP}$(ppm)	106	1.85 ± 0.07	19.7 ± 1.3	24.8 ± 1.7
3	0.24 ± 0.12				

$htt^{NT}Q_7P_{11}K_2$

Residue	^{15}N-$\Delta\omega_{E_SP}$(ppm)	Residue	$^{13}C\alpha$-$\Delta\omega_{E_SP}$(ppm)	$^{13}C\alpha$-R_{2,E_SP}^{600MHz}(s^{-1})	$^{13}C\alpha$-R_{2,E_SP}^{800MHz}(s^{-1})
22	0.12 ± 0.01	P25-P33	-0.33 ± 0.02	20.2 ± 5.9	20.4 ± 4.9
23	0.18 ± 0.01	P34	-0.35 ± 0.02	15.0 ± 4.9	15.6 ± 5.8
35	0.07 ± 0.02				
36	0.17 ± 0.02				

Table S4. Residue-specific fitted values of ^{15}N-Δω and ^{15}N-R_2 obtained for the NT domain of ^{15}N-labeled htt^{ex1} in the presence of a saturating amount of unlabeled profilin.[a]

htt^{ex1} + Profilin		0.4 mM htt^{ex1}		0.75 mM htt^{ex1}	
Residue	^{15}N-$\left\|\Delta\omega_{E_2^*P}\right\|$ (ppm)	^{15}N-$R_{2,E_2^*P}^{600MHz}$ (s^{-1}	^{15}N-$R_{2,E_2^*P}^{800MHz}$ (s^{-1})	^{15}N-$R_{2,E_2^*P}^{600MHz}$ (s^{-1})	^{15}N-$R_{2,E_2^*P}^{800MHz}$ (s^{-1})
3	2.24 ± 0.12	7.9 ± 0.1	9.9 ± 0.1	10.1 ± 0.1	12.9 ± 0.1
4	3.18 ± 0.19	10.7 ± 0.1	14.5 ± 0.1	13.3 ± 0.1	18.7 ± 0.2
5	2.00 ± 0.08	10.6 ± 0.1	13.4 ± 0.1	12.6 ± 0.1	15.8 ± 0.1
7	2.47 ± 0.10	12.0 ± 0.1	15.3 ± 0.1	13.7 ± 0.1	17.7 ± 0.3
8	2.31 ± 0.10	12.1 ± 0.1	15.3 ± 0.1	13.6 ± 0.1	18.3 ± 0.1
9	1.46 ± 0.08	13.1 ± 0.1	16.2 ± 0.1	14.2 ± 0.1	18.1 ± 0.1
10	1.13 ± 0.09	12.2 ± 0.1	15.3 ± 0.1	13.4 ± 0.1	16.3 ± 0.1
11	2.87 ± 0.12	14.2 ± 0.1	18.7 ± 0.1	16.2 ± 0.1	20.9 ± 0.2
12	1.44 ± 0.08	12.5 ± 0.1	15.4 ± 0.1	13.4 ± 0.1	16.4 ± 0.1
14	1.41 ± 0.08	14.2 ± 0.1	17.7 ± 0.1	15.3 ± 0.1	18.9 ± 0.1
15	1.65 ± 0.08	13.7 ± 0.1	16.8 ± 0.1	14.6 ± 0.1	17.8 ± 0.1

[a]Note that the sign of ^{15}N-Δω cannot be defined by the ^{15}N-CPMG data alone.

SI References

1. A. Ceccon, V. Tugarinov, G. M. Clore, (2018) TiO_2 nanoparticles catalyze oxidation of huntingtin exon 1-derived peptides impeding aggregation: a quantitative NMR study of binding and kinetics. *J Am Chem Soc* 141(1):94-97.
2. S. A. Kotler *et al*., (2019) Probing initial transient oligomerization events facilitating Huntingtin fibril nucleation at atomic resolution by relaxation-based NMR. *Proc Natl Acad Sci U S A* 116(9):3562-3571.
3. P. Lundstrom *et al*., (2007) Fractional ^{13}C enrichment of isolated carbons using [1-^{13}C]- or [2-^{13}C]-glucose facilitates the accurate measurement of dynamics at backbone Calpha and side-chain methyl positions in proteins. *J Biomol NMR* 38(3):199-212.
4. S. Chen, R. Wetzel, (2001) Solubilization and disaggregation of polyglutamine peptides. *Protein Sci* 10(4):887-891.
5. E. Rennella, A. Sekhar, L. E. Kay, (2017) Self-assembly of human profilin-1 detected by Carr-Purcell-Meiboom-Gill nuclear magnetic resonance (CPMG NMR) spectroscopy. *Biochemistry* 56(5):692-703.
6. H. Zhao, C. A. Brautigam, R. Ghirlando, P. Schuck, (2013) Overview of current methods in sedimentation velocity and sedimentation equilibrium analytical ultracentrifugation. *Curr Protoc Protein Sci* Chapter 20(Unit20 12.
7. H. Zhao *et al*., (2013) Recorded scan times can limit the accuracy of sedimentation coefficients in analytical ultracentrifugation. *Anal Biochem* 437(1):104-108.
8. R. Ghirlando *et al*., (2013) Improving the thermal, radial, and temporal accuracy of the analytical ultracentrifuge through external references. *Anal Biochem* 440(1):81-95.
9. P. Schuck, (2000) Size-distribution analysis of macromolecules by sedimentation velocity ultracentrifugation and lamm equation modeling. *Biophys J* 78(3):1606-1619.
10. J. L. Cole, J. W. Lary, P. M. T, T. M. Laue, (2008) Analytical ultracentrifugation: sedimentation velocity and sedimentation equilibrium. *Methods Cell Biol* 84(143-179.
11. F. Delaglio *et al*., (1995) NMRPipe: a multidimensional spectral processing system based on UNIX pipes. *J Biomol NMR* 6(3):277-293.
12. J. Ying, F. Delaglio, D. A. Torchia, A. Bax, (2017) Sparse multidimensional iterative lineshape-enhanced (SMILE) reconstruction of both non-uniformly sampled and conventional NMR data. *J Biomol NMR* 68(2):101-118.
13. D. F. Hansen, P. Vallurupalli, L. E. Kay, (2008) An improved ^{15}N relaxation dispersion experiment for the measurement of millisecond time-scale dynamics in proteins. *J Phys Chem B* 112(19):5898-5904.
14. D. F. Hansen, P. Vallurupalli, P. Lundstrom, P. Neudecker, L. E. Kay, (2008) Probing chemical shifts of invisible states of proteins with relaxation dispersion NMR spectroscopy: how well can we do? *J Am Chem Soc* 130(8):2667-2675.
15. A. Ceccon, V. Tugarinov, A. Bax, G. M. Clore, (2016) Global dynamics and exchange kinetics of a protein on the surface of nanoparticles revealed by relaxation-based solution NMR spectroscopy. *J Am Chem Soc* 138(18):5789-5792.
16. D. S. Libich, N. L. Fawzi, J. Ying, G. M. Clore, (2013) Probing the transient dark state of substrate binding to GroEL by relaxation-based solution NMR. *Proc Natl Acad Sci U S A* 110(28):11361-11366.